From Trivial Kondo Insulator $Ce_3Pt_3Bi_4$ to Topological Nodal-Line Semimetal $Ce_3Pd_3Bi_4$

Chao Cao,[1,2,*] Guo-Xiang Zhi,[3] and Jian-Xin Zhu[4,†]
[1]Condensed Matter Group, Department of Physics, Hangzhou Normal University, Hangzhou 310036, People's Republic of China
[2]Center of Correlated Materials, Zhejiang University, Hangzhou 310058, China
[3]Department of Physics, Zhejiang University, Hangzhou 310013, People's Republic of China
[4]Theoretical Division and Center for Integrated Nanotechnologies, Los Alamos National Laboratory, Los Alamos, New Mexico 87545, USA

(Received 26 April 2019; revised manuscript received 1 March 2020; accepted 3 April 2020; published 22 April 2020)

Using the density functional theory combined with dynamical mean-field theory, we have performed systematic study of the electronic structure and its band topology properties of $Ce_3Pt_3Bi_4$ and $Ce_3Pd_3Bi_4$. At high temperatures (~290 K), the electronic structures of both compounds resemble the open-core $4f$ density functional calculation results. For $Ce_3Pt_3Bi_4$, clear hybridization gap can be observed below 72 K, and its coherent momentum-resolved spectral function below 18 K exhibits an topologically trivial indirect gap of ~6 meV and resembles density functional band structure with itinerant $4f$ state. For $Ce_3Pd_3Bi_4$, no clear hybridization gap can be observed down to 4 K, and its momentum-resolved spectral function resembles electron-doped open-core $4f$ density functional calculations. The band nodal points of $Ce_3Pd_3Bi_4$ at 4 K are protected by the gliding-mirror symmetry and form ringlike structure. Therefore, the $Ce_3Pt_3Bi_4$ compound is topologically trivial Kondo insulator while the $Ce_3Pd_3Bi_4$ compound is topological nodal-line semimetal.

DOI: 10.1103/PhysRevLett.124.166403

The electronic structure of strongly correlated systems is one of the most intriguing problems in condensed matter physics. Taking heavy fermion systems as an example, its electronic structure exhibits strong temperature dependence and Kondo effect, due to the subtle interplay between the hybridization of f electrons with the itinerant band electrons and strong Coulomb repulsion among the f electrons. Recently, there is renewed interest in these systems due to the discovery of electron band topology [1,2]. In addition to possible topological Kondo insulators (TKIs) [3,4], the possibility of Weyl Kondo semimetals WKSs has been brought up [5–9]. In particular, the proposal of a truly heavy-fermion WKS [5] has stimulated intensive theoretical and experimental studies [7–9]. Experimentally, the realization of a TKI-WKS phase transition from $Ce_3Pt_3Bi_4$ to $Ce_3Pd_3Bi_4$ has recently been hotly discussed [9–11]. In this Letter, using state-of-art first-principles method based on density functional theory (DFT) and its combination with dynamical mean-field theory (DMFT) [12–14], we show that the $Ce_3Pt_3Bi_4$ is a topologically trivial Kondo insulator; while $Ce_3Pd_3Bi_4$ is a topological nodal-line Kondo semimetal, which is protected by the nonsymmorphic symmetry of the crystal.

The DFT calculations were performed using the plane-wave projected augmented wave method as implemented in the VASP [15,16] code, and cross-checked with both the PWscf code [17] and the full-potential linearized augmented plane-wave (FP-LAPW) Wien2k code [18]. Experimental lattice parameters were used for both compounds [19,20]. The DMFT calculations were performed using the DMFTF package in connection with the Wien2k code [21], with $U = 6.0$ and $J = 0.7$ eV for Ce-$4f$ states. The continuous-time quantum Monte Carlo (CT-QMC) method was employed to solve the Anderson impurity problem [22], and charge-density self-consistency was achieved. For more details about the DFT and DMFT calculations, please refer to the Supplemental Material [23].

Both $Ce_3Pt_3Bi_4$ and $Ce_3Pd_3Bi_4$ compounds are body-centered cubic crystals with symmetry group $I\bar{4}3d$ (No. 220), which contains 6 gliding mirror symmetry operations. Our main results of $Ce_3Pt_3Bi_4$ are shown in Fig. 1. At high temperatures ($T = 290$ K), the Ce-$4f$ electrons are localized, leading to incoherent f bands near the Fermi energy E_F, while coherent conduction bands can still be identified between Γ-H, H-N, and P-H [Fig. 1(c)], thus the system is metallic. The spectral density shows two small humps near the Fermi level, formed by the Ce-$4f_{5/2}$ at E_F and Ce-$4f_{7/2}$ 380 meV above the Fermi energy, respectively. As the temperature is lowered to 72 K, the flat Ce-$4f_{5/2}$ band begins to form around 10 meV above E_F, which strongly hybridizes with the conduction bands. The spectral density shows a sharper Ce-$4f$ peak, but without any trace of hybridization gap at 72 K. At 36 K, the hybridization gap is already present, as the spectral density shows a clear dip

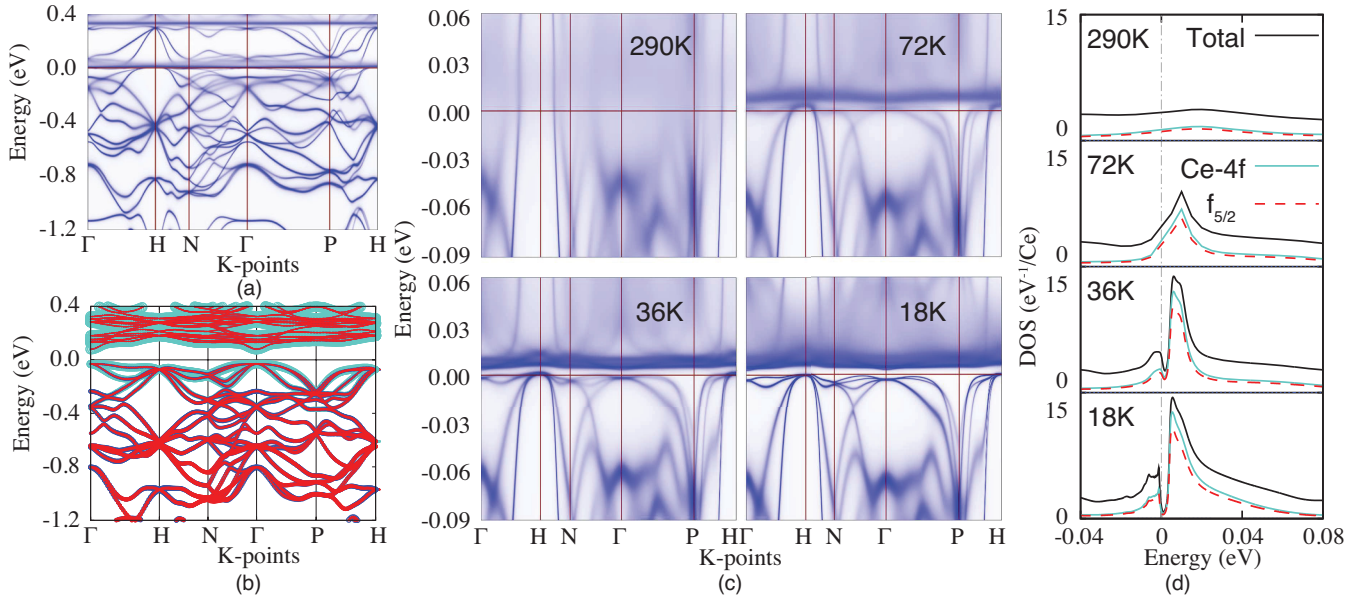

FIG. 1. Electronic structure of $Ce_3Pt_3Bi_4$. (a) The momentum-resolved spectral function from DFT + DMFT at 18 K. (b) The DFT band structure with itinerant Ce-4f states. The contributions from Ce-4f, Bi-6p, and Pt-5d states are represented by turquoise, blue, and red circles, respectively. (c) The DFT + DMFT momentum-resolved spectral functions at 290, 72, 36, and 18 K. (d) The DFT + DMFT spectral density at 290, 72, 36, and 18 K. The solid black line is the total spectral density, while the turquoise solid line, red dashed line, and blue dotted line represent Ce-4f, Ce-4$f_{5/2}$, and Ce-4$f_{7/2}$ contributions, respectively.

around the Fermi level E_F. At and below 36 K, the many-body self-energy of Ce-4$f_{5/2}$ states within the energy gap show a Fermi-liquid-like behavior $\mathrm{Im}[\Sigma_{5/2}(\omega)] \approx \alpha(\omega - \omega_0)^2 + \Sigma_0$ with a very small Σ_0 and ω_0 inside the gap (refer to Figs. S-2 and S-3 in Supplemental Material [23] for details), while such fitting is not possible at 72 K. Therefore, the coherence temperature is expected to be between 36 and 72 K from our calculation. Experimentally, the hybridization gap starts to form below 100 K, and its maximum value is measured to be approximately 50 K (or 4.3 meV) [24–28]. In addition, the momentum-resolved spectral function clearly shows an energy gap at E_F, and an indirect gap of ~6 meV can be identified from integrated and momentum-resolved spectral function plots at 18 K. In all these DFT + DMFT calculations, the Ce-4$f_{5/2}$ occupation ranges from around 1.00 at 290 K to 0.98 at 18 K, suggesting negligible valence fluctuation. Therefore, the system is consistent with the Kondo lattice model, where the f electrons can be treated as localized spins coupled to conduction electrons via a Kondo exchange interaction.

We notice that the coherent momentum-resolved spectral function at 18 K from DFT + DMFT calculation is indeed very similar to DFT results with itinerant Ce-4f states [Fig. 1(b)]. The DFT band structure yields an insulating ground state with ~140 meV indirect gap near Γ. The highest occupied state at Γ is the fourfold degenerate Γ_8 state in DFT calculation. It splits into two doubly degenerate states along the Γ-H line. At the H point, these four states are joined by the doubly degenerate state from Γ_7 at around 0.2 eV below E_F at Γ, as well as another doubly degenerate state stemming from the split Γ_8 state at ~0.4 eV below E_F, to form an eightfold degenerate state as the highest occupied state. This is exactly the same result we obtained for the coherent momentum-resolved spectral function at 18 K from DFT + DMFT calculations. Such analysis can be conducted along all high symmetry lines we presented, although the band energies are strongly renormalized in the DFT + DMFT calculations. The DFT calculation yields an insulating ground state with an indirect gap of ~140 meV, which is about 20 times larger than the DFT + DMFT result at 18 K. This is consistent with the mass enhancement factor $m^*/m \approx 26$ obtained from the many-body self-energy Σ.

The striking similarities between the DFT result and the DFT + DMFT result below the coherence temperature suggest that the coherent DFT + DMFT momentum-resolved spectral function can be adiabatically transformed from DFT result without closing the energy gap. Therefore, the topological properties of $Ce_3Pt_3Bi_4$ coherent spectral function from the DFT + DMFT is anticipated to be the same as its DFT band structure. It is worth noting that the global energy gap is already present in the calculations for $Ce_3Pt_3Bi_4$ even when the spin-orbit coupling is turned off (Supplemental Material [23], Fig. S-4a), and is therefore not related to the band inversion. Therefore, the $Ce_3Pt_3Bi_4$ is expected to be a Kondo insulator with trivial band topology. In fact, we have fitted the DFT band structure to a tight-binding Hamiltonian using the maximally localized Wannier function method [29] [refer to Supplemental Material [23], Fig. S-6(a)], and performed Wilson loop

calculations [30]. The resulting $\mathcal{Z}_2$ is (0;000) for $Ce_3Pt_3Bi_4$ [see Ref. [23] Fig. S-8(a)], showing its trivial topology nature. In addition, we have also employed the so-called topological Hamiltonian, i.e., inverse of the zero-frequency Green's function [31–34] to determine the same property for the correlated many-body Hamiltonian from DFT + DMFT. The resulting $\mathcal{Z}_2$ is also (0;000) as expected from the adiabatic argument [refer to Ref. [23] Fig. S-8(b)]. Therefore, the experimentally observed resistivity saturation must have an origin other than topological arguments, and robust surface states are not guaranteed. Indeed, the Hall measurement suggested the conduction of $Ce_3Pt_3Bi_4$ at low temperature is dominated by bulk in-gap states, unlike SmB_6, and is susceptible to low concentrations of disorders [28].

Having established that the $Ce_3Pt_3Bi_4$ is a trivial Kondo insulator, we now focus on the $Ce_3Pd_3Bi_4$ compound. The $Ce_3Pd_3Bi_4$ compound is isostructural to $Ce_3Pt_3Bi_4$ with nearly identical lattice constants and slightly different Bi atomic coordinates. It is therefore tempting to believe that the electronic structure of $Ce_3Pd_3Bi_4$ is similar to $Ce_3Pt_3Bi_4$. However, our DFT + DMFT calculations show that the temperature dependence of the $Ce_3Pd_3Bi_4$ electronic structure is very different (Fig. 2). At 290 K, the Ce-4f states are localized, as suggested by the highly dispersive quasiparticle conduction bands in Fig. 2(b). As the temperature is decreased, the Ce-4f flat band starts to form slightly above the Fermi level. However, they never form coherent Ce-4f states down to 4 K, indicated by its large imaginary part of self-energy close to the Fermi level (≈30 meV at 4 K; see also Supplemental Material [23], Figs. S-2 and S-3). The ligand state near the Fermi level, on the other hand, becomes sharp below 9 K. This is most prominent from the states between Γ-N (indicated by the red circles in Fig. 2, also in Supplemental Material [23], Fig. S-9) and Γ-P near E_F. During the whole temperature range, we do not observe a well-defined gap opening at the Fermi level down to 4 K in our calculation, thus $Ce_3Pd_3Bi_4$ is most likely to be a correlated metal at low temperatures and the Ce-4f electrons remain localized at low temperatures for $Ce_3Pd_3Bi_4$.

We now compare the DFT + DMFT momentum-resolved spectral function for $Ce_3Pd_3Bi_4$ at 4 K with DFT calculations treating the Ce-4f state as core electrons. Similar results can be obtained using LDA + U calculations with proper treatment of time-reversal symmetry [see Supplemental Material [23], Figs. S-5(c) and (d) for details]. Again, the momentum-resolved spectral function at 4 K for $Ce_3Pd_3Bi_4$ resembles the DFT results, if the Fermi level in the DFT band structure is shifted ∼0.2 eV higher [marked by the gray line in Figs. 3(a)–3(b)]. The DFT band structure has a large band gap of nearly 500 meV at approximately 1 eV above the Fermi level, or equivalent to counting 6 more electrons per unit cell. The states near E_F are dominated by Bi-6p and Ce-5d orbitals with a small

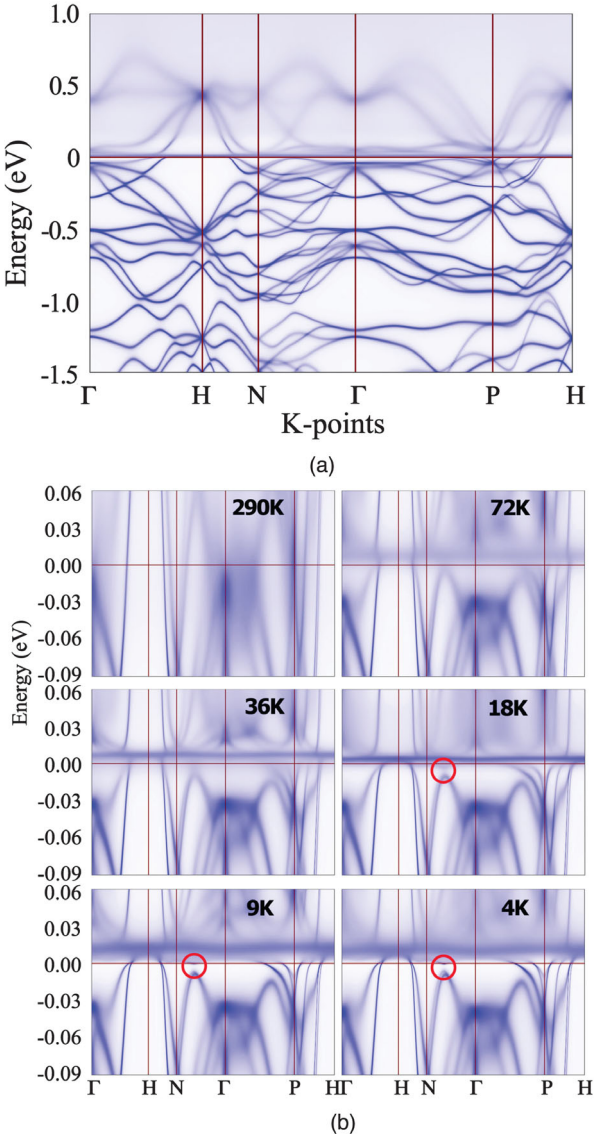

FIG. 2. Electronic structure of $Ce_3Pd_3Bi_4$. (a) The DFT + DMFT momentum-resolved spectral function in the energy range [−1.5,1.0] eV with respect to the Fermi energy at 4 K. (b) The DFT + DMFT momentum-resolved spectral function in an enlarged energy range close to the Fermi level at 290, 72, 36, 18, 9, and 4 K.

mixture of the Pd-4d orbitals. We note that the centers of gravity of the Pd-4d orbitals are located in the energy region between $[-4,-2]$ eV below E_F. The highest occupied states at Γ are doubly degenerate Γ_7, quarterly degenerate Γ_8 and doubly degenerate Γ_6 (from higher energy to lower energy), respectively. Along the Γ-H line, the Γ_8 states split into two doubly degenerate bands, and both Γ_6 and Γ_7 states remain doubly degenerate. The Γ_7 state and one pair of the split Γ_8 state are joined by other 2 doubly degenerate bands to form an eightfold degenerate highest occupied state at H. It again splits into 4 doubly degenerate states along H-N, and further splits into 8 singly degenerate states along N-Γ. Such splittings are all present

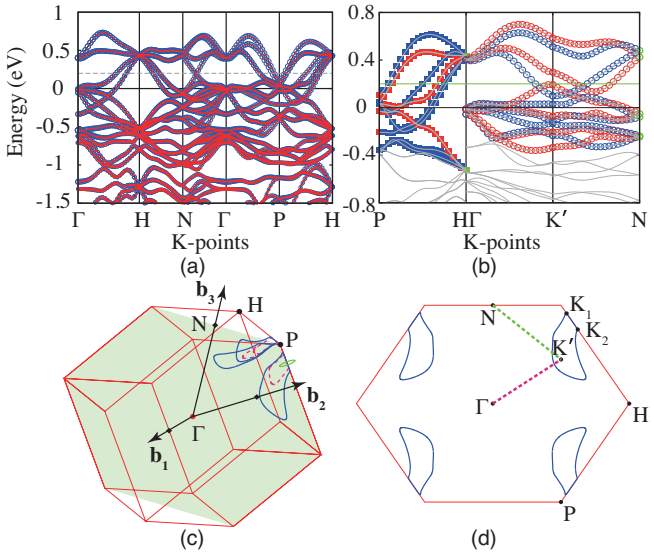

FIG. 3. DFT electronic structure of $Ce_3Pd_3Bi_4$. (a) The DFT band structure calculated by assuming an open-core Ce-4f state. The size of the red circles are proportional to the Pd-4d state contributions, while the blue circles are contributions from Ce-4f and Bi-6p states. (b) The band structure on the gliding mirror plane Γ-N-P. K' is (0, 1/4, 1/4). Along P-H, the bands can be classified with C_3 eigenvalues $e^{\pm i2\pi/3}$ (red squares) and 1 (blue squares). In other directions, the bands can be labeled with $-i$ (red circles) or i (blue circles). (c) The first Brillouin zone showing the high symmetry points and the nodal rings. The green circle is the path used to calculate the Berry phase. (d) The nodal rings (blue lines) on one of the gliding-mirror planes.

in 4 K momentum-resolved spectral functions from DFT + DMFT calculations.

Similar to our previous analysis for $Ce_3Pt_3Bi_4$, we argue that the similarity between the 4 K momentum-resolved spectral function and DFT band structure ensures that the topological properties of $Ce_3Pd_3Bi_4$ can be analyzed using the DFT results with proper Fermi level shifting. Judging from the bands crossing the Fermi level between N-Γ and around P, the DFT results can be compared with DFT + DMFT results [see also Supplemental Material [23] Fig. S-9(a)] if the DFT Fermi level is shifted upward by approximately 0.2 eV. In addition, the Fermi surface from open-core Ce-4f DFT calculations matches that from the DFT + DMFT calculations at 4 K after 0.2 eV Fermi level shifting, both of which consist of 4 sheets around H and 4 sheets around P points [Supplemental Material [23], Fig. S-10(a) and (c)]. On the contrary, the Fermi surface from open-core Ce-4f DFT calculations without Fermi level shifting consists of 2 sheets around H and 2 sheets around P points [Supplemental Material [23], Fig. S-10 (b)]. From the DFT DOS [Supplemental Material [23], Fig. S-7(b)], we found that 0.2 eV Fermi level shifting is equivalent to 1 electron doping per formula (or 2e per unit cell). Therefore, we need to locate for the nodal structures between band 4 and band 5 [band indices are marked on Supplemental Material [23] Fig. S-11(b)]. Notice that the crystal contains 6 gliding-mirror planes in $\{100\}$ and five other equivalent directions, the states in $k_x = k_y$ and all equivalent k planes can be classified using the mirror symmetry. Let us consider 1 of the 6 equivalent planes (η, ξ, ξ) (in crystal coordinate). First of all, there is a high symmetry line P-H within this plane, which is shared by other 2 gliding mirror planes. In addition to the gliding mirror symmetry, C_3 rotation symmetry is also preserved along this line. Therefore, all states can be labeled with C_3 eigenvalues $e^{\pm i2\pi/3}$ or 1, the former is doubly degenerate. At point P, bands 2–4 and 5–7 are triply degenerate due to the local T_d symmetry. As it moves along P-H, they both split into a singly degenerate band (4 and 7) and a pair of doubly degenerate band (2,3 and 5,6). Band 4 then crosses doubly degenerate band 5/6 twice, creating two triply degenerate points at K_1 (0.238, 0.254, 0.254) (all the coordinates are in direct unit, unless otherwise specified) and K_2 (0.046, 0.318, 0.318), as well as a segment of nodal line between them. It is also instructive to notice that bands 1–7 and 10 will join together at H and form an eightfold degenerate state; while bands 8–9 are doubly degenerate states and will be joined by other 6 states at H to form another eightfold degenerate state. Second, we take a look at another K path from Γ to the K' (0.0, 0.25, 0.25) point. As all these states are in the mirror plane, they can be labeled with $\pm i$. Evidently, there is a band inversion between the band 4 and 5 between the Γ and K' points, and therefore there must be a nodal point. In fact, such a nodal point can be identified between K' and any K point along Γ-P or Γ-H. Therefore, we conclude that these nodal points must form a nodal ring within the triangle Γ-H-P. Since there are 6 gliding-mirror planes, and each plane contains 4 such triangles within the first BZ, there are 24 nodal rings, forming 8 groups around 8 P points, each group contains 3 nodal rings sharing the same K_1-K_2 nodal line. The Berry phase around a circular path perpendicular to P-H around the K_1-K_2 nodal line is π or -π, indicating its nontrivial topology. In the open-core Ce-4f electron DFT calculations, these nodal rings occupy energy ranges from 0.1 to 0.3 eV above E_F, therefore they cross the Fermi level if the Fermi level is shifted 0.2 eV upward (1e doping per formula). In the DFT + DMFT calculations, these nodal rings can also be identified in the momentum-resolved spectral function at 4 K. From P-H, the doubly degenerate states 5/6 are not very sharp a few meVs below E_F. However, such crossings can still be identified at ~50 meV below E_F. We have also employed the topological Hamiltonian method to determine the nodal structure of $Ce_3Pd_3Bi_4$ at 4 K. These results are shown in Fig. 3(c) with dashed magenta lines. The topological Hamiltonian yields nodal rings similar to the open-core DFT calculations, but the size of these rings are much reduced due to the many-body renormalization effect. In addition to the 24 nodal rings we described above, we have also identified band

crossings at 6 H points, as well as at 24 points at (0.328, 0.153, 0.000) (in cartesian coordinates, $Å^{-1}$ unit) and its symmetrically equivalent positions. However, the chirality of all these crossings are 0, meaning that they are not topological.

An important question is what leads to the difference between $Ce_3Pt_3Bi_4$ and $Ce_3Pd_3Bi_4$ compounds. Since Pt and Pd belong to the same element family, and both compounds are isostructural with nearly identical lattice constants, the spin-orbit coupling (SOC) change seems to be one very plausible reason. However, if we compare the band states in the energy range $[-0.5, 1.0]$ eV in the DFT calculations by assuming open-core Ce-4f electrons (Supplemental Material [23], Fig. S-5), it is clear that the $Ce_3Pt_3Bi_4$ SOC splitting near E_F is not very different from $Ce_3Pd_3Bi_4$. From the DFT calculations, the spin-orbit coupling constants λ_{SO} are 0.453/0.659/1.051 eV for Ce/Pt/Bi atoms in $Ce_3Pt_3Bi_4$, and 0.454/0.324/1.074 eV for Ce/Pd/Bi atoms in $Ce_3Pd_3Bi_4$, respectively. More importantly, we notice that the $Ce_3Pd_3Bi_4$ compound would also be an insulator with a large band gap in the DFT calculations if Ce-4f electrons are treated as being itinerant. Therefore, such a difference is more likely related to a change in hybridization. In fact, the hybridization function Δ for $4f_{5/2}$ exhibits completely different behavior for $Ce_3Pt_3Bi_4$ and $Ce_3Pd_3Bi_4$. If we compare the imaginary part of $\Delta_{f5/2}$ in the Matsubara frequency domain for both compounds at 18 K (please refer to Supplemental Material [23], Fig. S-12a), it is clear that $\mathrm{Im}[\Delta_{f5/2}]$ for $Ce_3Pt_3Bi_4$ blows up below $\omega_n = 40$ meV, consistent with a Kondo insulator behavior [35]; while for $Ce_3Pd_3Bi_4$, $\mathrm{Im}[\Delta_{f5/2}]$ remains finite and reduces in the same frequency range. Correspondingly, the hybridization function in real-frequency axis $\Delta(\omega)$ exhibits singular peaks at the Fermi level for $Ce_3Pt_3Bi_4$; while such peaks are absent for $Ce_3Pd_3Bi_4$ [see also Supplemental Material [23] Fig. S-12(b)].

In conclusion, we have performed a systematic DFT and DFT + DMFT study of $Ce_3Pt_3Bi_4$ and $Ce_3Pd_3Bi_4$ compounds. The $Ce_3Pt_3Bi_4$ compound is a trivial Kondo insulator with an indirect gap of ~6 meV. The $Ce_3Pd_3Bi_4$ compound is a correlated metal with topological nodal lines at low temperatures. The hybridization change is the main driving force for the above-mentioned transition.

The authors are grateful to Qimiao Si, S. K. Kushwaha, P. F. S. Rosa, N. Harrison, J. Lawrence, Huiqiu Yuan, Jianhui Dai, and Frank Steglich for stimulating discussions. C. C. also acknowledges the hospitality of Los Alamos National Laboratory, where this work was initiated. This work at Los Alamos was carried out under the auspices of the U.S. Department of Energy (DOE) National Nuclear Security Administration under Contract No. 89233218CNA000001. It was supported by NSFC 11874137 and 973 Project 2014CB648400 (C. C. and G.-X. Z.), and U.S. DOE BES under LANL-E3B5 and, in part, by Center for Integrated Nanotechnologies, a DOE BES user facility, in partnership with LANL IC Program for computational resources (J.-X. Z.). The calculations were performed also on the High Performance Computing Cluster of Center of Correlated Matters at Zhejiang University, and Tianhe-2 Supercomputing Center.

*ccao@hznu.edu.cn
†jxzhu@lanl.gov

[1] M. Z. Hasan and C. L. Kane, Rev. Mod. Phys. **82**, 3045 (2010).
[2] X.-L. Qi and S.-C. Zhang, Rev. Mod. Phys. **83**, 1057 (2011).
[3] D. J. Kim, J. Xia, and Z. Fisk, Nat. Mater. **13**, 466 (2014).
[4] P.-Y. Chang, O. Erten, and P. Coleman, Nat. Phys. **13**, 794 (2017).
[5] H.-H. Lai, S. E. Grefe, S. Paschen, and Q. Si, Proc. Natl. Acad. Sci. U.S.A. **115**, 93 (2018).
[6] C. Guo, C. Cao, M. Smidman, F. Wu, Y. Zhang, F. Steglich, F.-C. Zhang, and H. Yuan, Quantum Mater. **2**, 39 (2017).
[7] P.-Y. Chang and P. Coleman, Phys. Rev. B **97**, 155134 (2018).
[8] C. Y. Guo, F. Wu, Z. Z. Wu, M. Smidman, C. Cao, A. Bostwick, C. Jozwiak, E. Rotenberg, Y. Liu, F. Steglich *et al.*, Nat. Commun. **9**, 4622 (2018).
[9] S. Dzsaber, L. Prochaska, A. Sidorenko, G. Eguchi, R. Svagera, M. Waas, A. Prokofiev, Q. Si, and S. Paschen, Phys. Rev. Lett. **118**, 246601 (2017).
[10] S. Dzsaber, X. Yan, G. Eguchi, A. Prokofiev, T. Shiroka, P. Blaha, O. Rubel, S. E. Grefe, H.-H. Lai, Q. Si *et al.*, arXiv:1811.02819.
[11] S. Kushwara, M. K. Chan, J. Park, S. Thomas, E. D. Bauer, J. Thompson, F. Ronning, P. F. Rosa, and N. Harrison, Nat. Commun. **10**, 5487 (2019).
[12] A. Georges, G. Kotliar, W. Krauth, and M. J. Rozenberg, Rev. Mod. Phys. **68**, 13 (1996).
[13] G. Kotliar, S. Y. Savrasov, K. Haule, V. S. Oudovenko, O. Parcollet, and C. A. Marianetti, Rev. Mod. Phys. **78**, 865 (2006).
[14] E. Gull, A. J. Millis, A. I. Lichtenstein, A. N. Rubtsov, M. Troyer, and P. Werner, Rev. Mod. Phys. **83**, 349 (2011).
[15] G. Kresse and J. Hafner, Phys. Rev. B **47**, 558 (1993).
[16] G. Kresse and D. Joubert, Phys. Rev. B **59**, 1758 (1999).
[17] P. Giannozzi, O. Andreussi, T. Brumme, O. Bunau, M. B. Nardelli, M. Calandra, R. Car, C. Cavazzoni, D. Ceresoli, M. Cococcioni *et al.*, J. Phys. Condens. Matter **29**, 465901 (2017).
[18] K. Schwarz, P. Blaha, and G. K. H. Madsen, Comput. Phys. Commun. **147**, 71 (2002).
[19] G. H. Kwei, J. M. Lawrence, P. C. Canfield, W. P. Beyermann, J. D. Thompson, Z. Fisk, A. C. Lawson, and J. A. Goldstone, Phys. Rev. B **46**, 8067 (1992).
[20] W. Hermes, S. Linsinger, R. Mishra, and R. Pöttgen, Monatsh. Chem. **139**, 1143 (2008).
[21] K. Haule, C.-H. Yee, and K. Kim, Phys. Rev. B **81**, 195107 (2010).
[22] K. Haule, Phys. Rev. B **75**, 155113 (2007).
[23] See Supplemental Material at http://link.aps.org/supplemental/10.1103/PhysRevLett.124.166403 for additional calculation information.

[24] B. Bucher, Z. Schlesinger, P. C. Canfield, and Z. Fisk, Phys. Rev. Lett. **72**, 522 (1994).
[25] M. F. Hundley, P. C. Canfield, J. D. Thompson, Z. Fisk, and J. M. Lawrence, Phys. Rev. B **42**, 6842 (1990).
[26] A. Severing, J. D. Thompson, P. C. Canfield, Z. Fisk, and P. Riseborough, Phys. Rev. B **44**, 6832 (1991).
[27] J. C. Cooley, M. C. Aronson, and P. C. Canfield, Phys. Rev. B **55**, 7533 (1997).
[28] N. Wakeham, P. F. S. Rosa, Y. Q. Wang, M. Kang, Z. Fisk, F. Ronning, and J. D. Thompson, Phys. Rev. B **94**, 035127 (2016).
[29] I. Souza, N. Marzari, and D. Vanderbilt, Phys. Rev. B **65**, 035109 (2001).
[30] R. Yu, X. L. Qi, A. Bernevig, Z. Fang, and X. Dai, Phys. Rev. B **84**, 075119 (2011).
[31] Z. Wang and S.-C. Zhang, Phys. Rev. X **2**, 031008 (2012).
[32] Z. Wang, X.-L. Qi, and S.-C. Zhang, Phys. Rev. B **85**, 165126 (2012).
[33] Z. Wang and S.-C. Zhang, Phys. Rev. X **4**, 011006 (2014).
[34] Z. Wang and B. Yan, J. Phys. Condens. Matter **25**, 155601 (2013).
[35] J. M. Tomczak, J. Phys. Condens. Matter **30**, 183001 (2018).